 CMES, vol.92, no.6, pp.557-571, 2013

Fracture Behavior of Heat Affected Zone of Laser-welded Joint for Ti-6Al-4V titanium alloy: Experimental and Computational Study

Zhao Xilong[1], **Zhang Jianxun**[1], **Chen Hongyuan**[1,2], **Song Xu**[1]

Abstract: In order to study failure perspective of Ti-6Al-4V titanium alloy welded joint, fracture behavior of the heat affected zone is researched. Microhardness, tensile test and microstructure are used to study the mechanical properties of the titanium alloy laser welded joint. The tensile and microhardness results show that heat affected zone near the base metal is the weakest in welded joints. This paper is based on the results from in-situ tension test to observe the process of crack expansion in heat affected zone. And then, in-situ test is simulated via the finite element method on ABAQUS Standard; therefore the fracture criteria are generated by comparing the applied force between simulation and in-situ test. Meanwhile, the GTN model is used to describe the damage behavior of the titanium alloy. The grain structure is simplified as voronoi convex polyhedron. And then, based on the in-situ test and its simulation, we conduct research on the fracture driving force under micro-scale condition. The simulation result indicates that the driving forces for metal fracture are jointly from the normal stress and shear stress.

Keywords: Simulation; fracture; finite element analysis; scanning electron microscopy

1 Introduction

With the constant progress of aviation and aerospace technologies, mechanical characteristics of titanium alloy and its joints under room temperature and high temperature have been studied widely [Squillace, Prisco and Ciliberto (2012)]. Researchers conducted research on the super-plasticity of titanium alloy under high temperature [Lee, Yoon and Park (2007)], and the impact of the size differences of grains on its mechanical characteristics [Patankar, Escobedo and Field (2002)], as

[1] State key laboratory for mechanical behavior of materials, Xi'an Jiaotong University, Xi'an 710049, China.
[2] Tubular Goods Research Institute of China National Petroleum Corporation, Xi'an 710049, China.

well as the effect of the strain rate under ultra-high temperature on its mechanical characteristics [Osovski, Nahmany and Rittel (2012)]. As Chan K.S found when conducting research on TiAl alloy, the fracture pattern of the equiaxed γ alloy was as follows: the micro-cracks and main cracks were interlinked, and then expanded till they eventually cause fracture [Chan and Kim (1995)]. When studying the slice layer structure of Ti-46.3AI-2V-1Cr alloy, Chen J. H found that the fracture driving force was normal stress [Chen, Cao and Wang (2004)].

In welding process, as heating mode and cooling rate vary, grain size and microstructure of each area in the welding joint vary as well. This has great impact on the mechanical characteristics of the welded joints. With infrared imaging method, Gao X.L conducted research on the variations of the material temperature field caused by failure of the titanium alloy laser-welded joint during the stretching process under the room temperature [Gao, Zhang and Liu (2013)]. Under the load changing condition, Zhang J.X conducted research on the internal damage behavior of different micro zones of the titanium alloy laser welded joints. And the result indicated that under the condition of low stress, the variation along the distance from the welded center line was not sharply different, while under the condition of high stress, the damage level close to the heat affected zone was evidently higher than that of other areas [Zhang, Song and Zheng (2012)]. Zhao X.L adopted the approach of shear punch test to research the difference between the mechanical performance in micro zones of the Ti6A14V titanium alloy laser welded joints; meanwhile, the in-situ test was conducted to observe the crack initiation in all micro zones of the titanium alloy laser welded joints and the variation of its crack expansion behavior [Zhao, Zhang and Song (2012); Zhao, Zhang and Guo (2011)]. However, as for the crack initiation in the weak area of the titanium alloy welded joints and the cause of its failure, and especially the critical criteria that cause the failure of the whole joints and even the over-all structure still cannot be described qualitatively.

Aiming at these issues, the plate of Ti-6Al-4V titanium alloy is welded by CO2 laser device. The microhardness test is used to find the weakest area in welded joints. And then, we take the in-situ test to observe the fracture behavior of heat affected zone in the joint. Meanwhile, a computing model of voronoi convex polyhedron is built in ABAQUS to simulate the microstructure model for studying the crack initiation and fracture criteria.

2 Experimental procedure

Rolled Ti6Al4V titanium alloy is used in the experiment, which is welded by CO2 laser device. The dimensions of the plate are 170 mm $\times$ 330 mm $\times$ 2.5 mm. The composition is shown as Table.1. And welding parameters are listed as: the power of laser is 2500 W, the defocusing amount is 0, and the welding speed is 1.5 m/min. After welding, vickers microhardness measurements are done on the base metal, heat affected zone and welded metal by a diamond pyramid indenter under a load of 300 gf with a dwelling time of 15 seconds. In addition, tensile sample is shown in Fig.1. Tensile testing is performed at room temperature on CSS-88100 universal tensile tester with a tension speed of 0.1 mm/min. A specimen notched in heat affected zone was observed by in situ. According to our previous research, the stand deviation of the specimen notched in HAZ is 6.117 [Zhao, Zhang and Song (2013)].

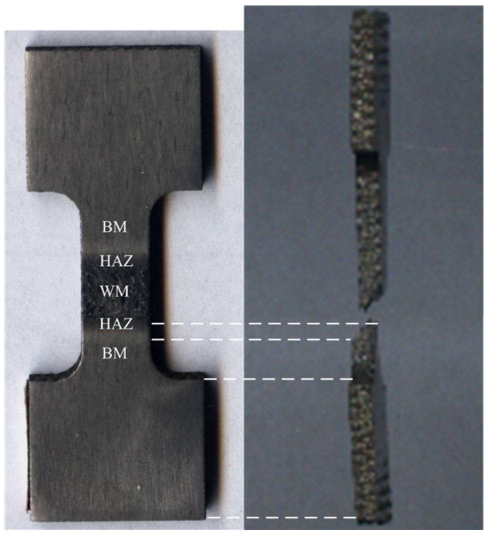

Figure 1: A view of joints welded by laser device before and after tension test

Table 1: Chemical composition of the titanium alloy Ti-6Al-4V(wt %)

Element	Al	V	Fe	Si	C	N	H	O
Content	5.5∼6.8	3.5∼4.5	≤ 0.3	≤ 0.15	≤ 0.1	≤ 0.05	≤ 0.015	≤ 0.2

3 Description of finite element model

The computational study of this work mainly involved simulation of cracks in macro-scale as well as micro-scale structures. For fracture mechanics, a new method named XFEM (Extended Finite element Method), which was first studied [Moës, Dolbow and Belytschko (1999); Belytschko and Black (1999)], got more popular in the past decade. It was an extension of the conventional finite element method based on the concept of partition of unity by [Melenk and Babuska (1996)]. Since then many studies have been devoted to XFEM. Recently, the SGBEM-FEM alternating method was compared systematically with the XFEM by [Dong and Atluri (2013a); Dong and Atluri (2013b)]. This method (SGBEM-FEM) could increase the accuracy for the computed stress intensity factors by coarse meshes, which could reduce the computation time. For microscopic mechanical properties, a usual way that was to use ABAQUS or other commercial finite element soft wares to model a RVE (Representative Volume Element) [Christman, Needleman and Suresh (1989), Bao, Hutchinson, McMeeking(1991)]. Meanwhile, a new method named T-Treffz Voronoi Cell Finite Elements (VCFEM-TTs), which were efficient and accurate for micromechanical study [Dong and Atluri(2011); Dong and Atluri(2012a); Dong and Atluri (2012b)]. In this paper, ABAQUS was used to simulate the in-situ test finite element model (section 3.1) and the polycrystal finite element model (section 3.3).

3.1 In-situ test finite element model

Based on the above-mentioned test result, 3D finite element model of in-situ test is developed using **ABAQUS Standard**. As shown in Fig.2, specimen mesh is set by C3D8R: 8-node hexahedron element with reduced integration and hourglass control. The uneven grids that are fine near the notch and coarse far from the notch are meshed. The size of the key area is 0.001 mm $\times$ 0.004 mm $\times$ 0.002 mm. The specimen model contains 27205 eight-node elements. The in-situ test is observed with tension speed of 0.1 mm/min. The keywords (Enrichment and TYPE is Stationary Crack) in **ABAQUS Standard** are used to study the in-situ method. Meanwhile, the special characteristic points are picked up from the in-situ test to finite element model, as shown in Fig.2. Some material parameters of Ti6Al4V titanium alloy are obtained from Ref [Zhang and Zhang (2009)], such as E= 116 000, MPa, μ= 0.3, and σ_s= 987 MPa. At last, the mechanical behavior in the enriched elements in the global model is discussed. The maximum principal stress failure criterion is selected for damage initiation; the GTN damage model is also selected in the model (except ***Porous Failure Criteria**). The parameters are described in section 3.2. The comparison of applied force between simulation and experiment is introduced in section 4.2.

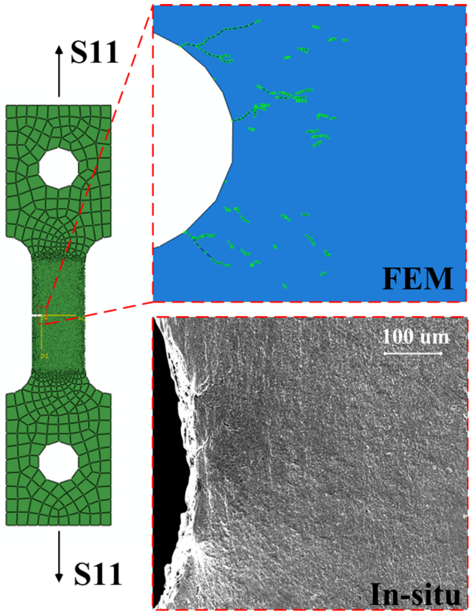

Figure 2: Finite element model of in-situ tension test

3.2 GTN model

Following the formulation given in Ref [Gurson (1977)], the yield surface of the GTN model was given by

$$F(\sigma_e,\sigma_m)=(\frac{\sigma_e}{\sigma_M})^2+2q_1 f^*\cosh(\frac{3q_2}{2}\frac{\sigma_m}{\sigma_M})-(1+q_3 f^{*2}) \tag{1}$$

Where q_1, q_2 and q_3 were the fitting parameters proposed by Tvergaard [Tvergaard and Needleman (1984); Needleman and Tvergaard (1984)]. The current state was characterized by f^*, a function of the void volume fraction f, yield stress of the undamaged matrix material σ_M, the hydrostatic pressure σ_m, and the von mises effective stress σ_e.

The stress triaxiality is defined as

$$T=\frac{\sigma_m}{\sigma_e} \tag{2}$$

The function f^* was given as

$$f^*=\begin{cases} f & f\le f_c \\ f_c+\frac{\overline{f_f}-f_c}{f_f-f_c}(f-f_c)......f_c<f<f_f,\overline{f_f}=\frac{q_1+\sqrt{q_1^2-q_3}}{q_3} & \\ \overline{f_f} & f\ge f_f \end{cases} \tag{3}$$

In the above relation, f_c was the critical value of void volume fraction and f_f was the void volume fraction at failure.

For the initial void volume fraction f_0, is calculated using optical microscope as shown in Fig.3. According to the previous research [Zhang, Song and Zheng (2012)], f_c is set to 0.005 as shown in Fig.4. And its statistical value is 0.00058. And fracture void volume fraction f_f is set to 0.08 empirically. Taking reference of our previous research [Zhang, Song and Zheng (2012); Zhao and Zhang (2013)] and others works [ABAQUS Theory Manual (1998); Hauert, Rossoll and Mortensen (2010)], the other value of parameters of the GTN model are: q_1=1.5; q_2=1; q_3=q_1^2=2.25; f_0=0.00058; f_f=0.08; f_c=0.005; ε_N=0.3; S_N=0.1.

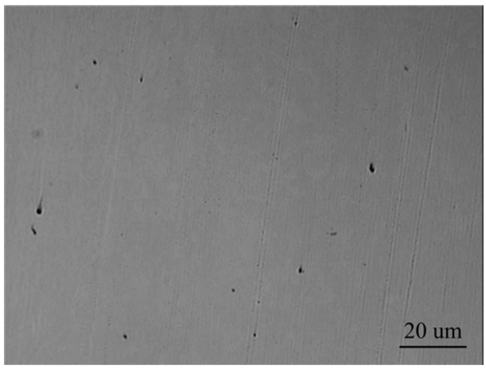

Figure 3: Initial void volume fraction of T6Al4V titanium alloy is determined by experiment

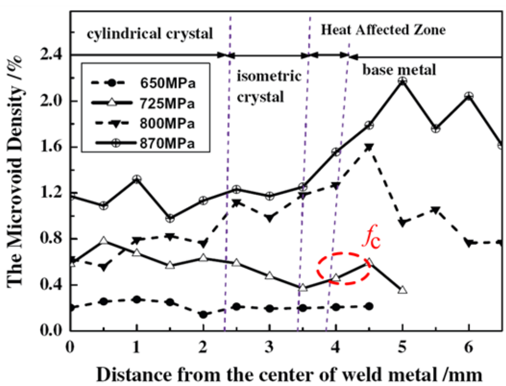

Figure 4: Microvoid density from weld center to base metal under different loads [Zhang, Song and Zheng (2012)]

3.3 Polycrystal finite element model

Based on the structure character of the heat affected zone, create a 40 μm×40 μm×40 μm RVE, which is simulated in **ABAQUS Explicit**. As shown in Fig.5, the model contains 30 grains. Finite element model mesh of each crystal uses the high-precision rectangular unit. Element type is set by C3D4: 4-node tetrahedron element with hourglass control. The ploycrystal model contains 29237 four-node elements. The GTN model is also used as material properties of each grain in RVE, which is discussed in section 3.2. Meanwhile, contact relationships of each grain are simplified as hard contact. The boundary condition is based on the in-situ tensile test and its simulation.

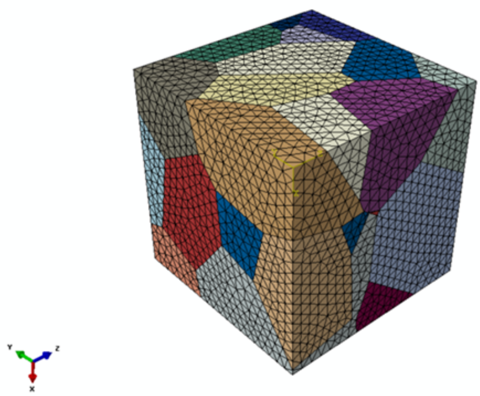

Figure 5: Finite element model of polycrystal model

4 Results and Discussion

4.1 Microstructure and microhardness

The microhardness test is performed on the whole welded joint and the result is shown in Fig.6. It can be seen that the HV of WM is somewhat higher than that of other areas, which is caused by imparity distribution of the Martensite (M) phase due to the rapid cooling rate. Meanwhile, there are some differences in the microhardness values in different zones of the base metal. The phenomenon is caused by rolling. However, HV of HAZ near the BM is the lowest in welded joints. The grain size of M phase is about 200∼300 μm in WM and about 5∼50 μm in HAZ respectively. There are β phase existing in HAZ near BM. The grain size of α

phase and β phase is 3$\sim$5 μm in BM and the microstructure of each area in the welded joint are shown in Fig.7a-d.

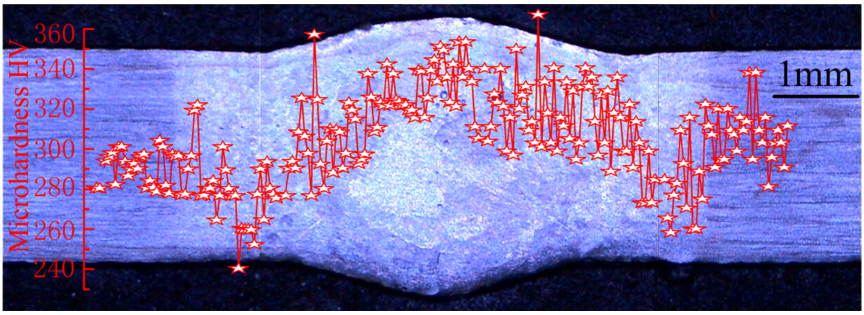

Figure 6: Microhardness of Ti-6Al-4V titanium alloy laser welded joints

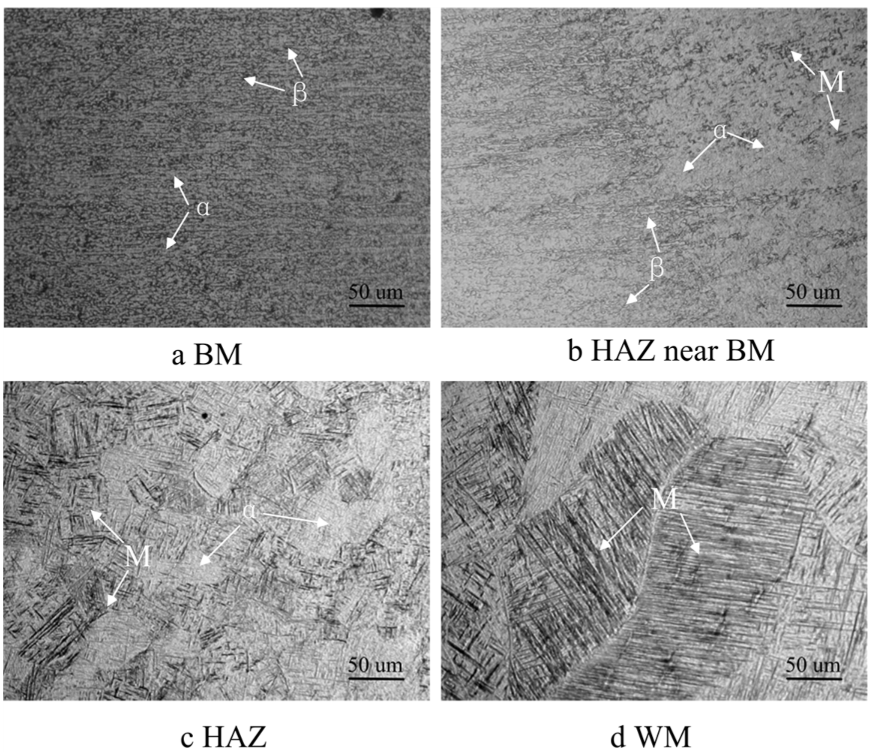

Figure 7: Microstructure of Ti-6Al-4V titanium alloy laser welded joints. (a) BM, (b) HAZ near BM, (c) HAZ, (d) WM.

4.2 Simulation of in-situ tensile test

The load and displacement curve and the crack expansion behavior generated by the in-situ tension test are shown in Fig.8. In Fig.8a, there are three characteristic points in the load-displacement curve of in-situ tensile test. Scanning electron microscope images of the three characteristic points are illustrated in Fig.8b. In Fig.8b it can be concluded that, when the specimen is at 1597 N, three crack origins appear at the front of the notch. With the load continuously increasing, the micro cracks show different level of expansion at these three crack origins. When the load increases to 1638 N, the eventual fracture failure occurs in the upper crack area.

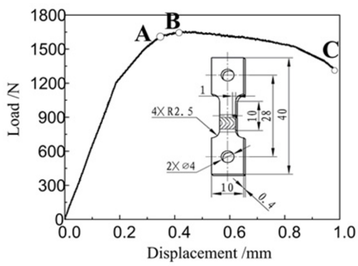

(a) Load displacement curve of in situ tension test

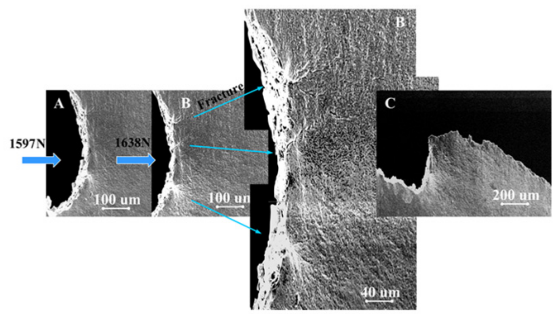

(b) Micrographs showing the evolution of the fracture process of in situ tension test

Figure 8: In situ tension test in the HAZ (a) Load displacement curve of in situ tension test, (b) the process of in situ tension test

The stress field at the crack tips generated by the finite element model simulation through the in-situ tension test is shown in Fig.9. The stress concentration amount of the upper crack tip at the front of the notch is evidently higher than the other two areas. The cause of this phenomenon may be the following: the occurrence of tiny cracks at the middle and bottom crack origins tips have absorbed large amount of energy, while at the tip of the main crack of upper area there are no tiny crack appearing. The variables of the three caracks are shown in table.2. The S11 stress values at the tip of the three cracks are as below: 1375 MPa at the upper crack, 1039 MPa at the middle crack, and 1241 MPa at the bottom crack. It can be concluded that the stress value at the tip of the upper crack is obviously higher than that of the middle crack and the bottom crack. The strain ε_{11} at the tip of three cracks are different. When at the tip of the upper crack, the strain value is 0.136, which is evidently higher than that of the middle crack which is 0.125, and that of the bottom crack which is 0.134. Meanwhile, the calculation results on the stress concentration of three cracks tip show that the stress triaxiality at the tip of the upper is 2.33, which is remarkably higher than that in middle crack tip (1.72) and that in bottom crack tip (2.13). According to the material failure criteria presented by Rice and the relevant revised theory presented by Chen J.H that the crack initiation are caused by the stress triaxiality [Chen, Wang and Wang (2003); Wang, Liu and Chen (2004)], it is easy to conclude that the critical fracture criterion for the titanium alloy at the heat affected zone is the following: the critical stress is 1375 MPa; the critical fracture strain is 0.136; and the critical stress triaxiality is 2.33.

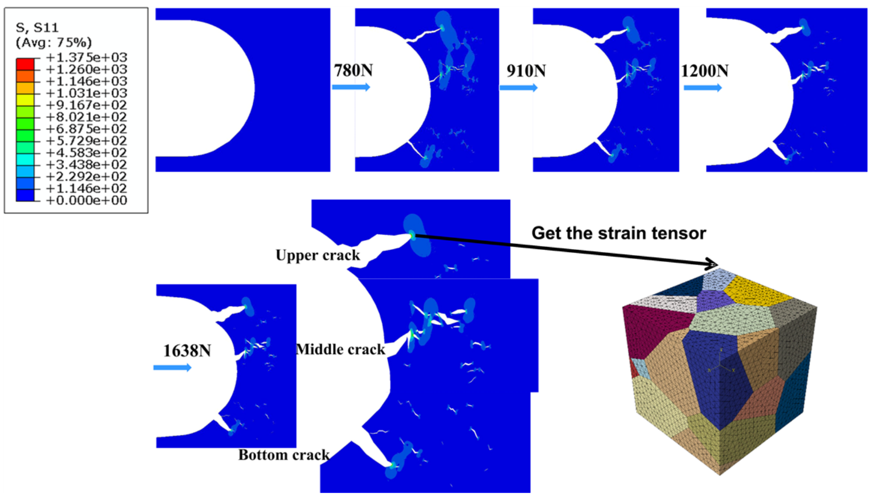

Figure 9: Finite element simulation of the in-situ test in the HAZ

Table 2: Chemical composition of the titanium alloy Ti-6Al-4V(wt %)

Variable Location	S11	critical fracture strain	stress triaxiality
Upper crack	1375 MPa	0.136	2.33
Middle crack	1039 MPa	0.125	1.72
Bottom crack	1241 MPa	0.134	2.13

4.3 Simulation of in-situ tensile test

In the mean time, the detailed values of the strain in front of upper crack are extracted. And then, the boundary condition of the polycrystal finite element model is that the strain tensor of the upper crack tip is from the time 0 s (in-situ test load is 0 N) to the time 173 s (in-situ test load is 1638 N). Here it is necessary to emphasize that the strain tensor is not input into ABAQUS directly, so an alternative approach is taken to indicate the strain via the relationship between the temperature and the thermal expansion coefficient. This method is widely used when Murakawa [Murakawa, H.; Deng and Ma (2011); Wang, Zhang and Serizawa (2009)] and Ueda's [Ueda, Yuan and Mochizuki (1993)] inherent strain theory is used as alternative strain loading method in other commercial finite element programs.

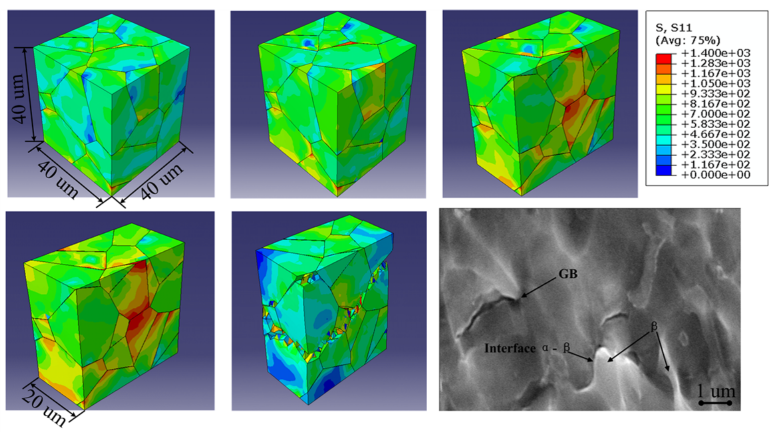

Figure 10: Finite element model in mesoscopic scale and its experimental verification

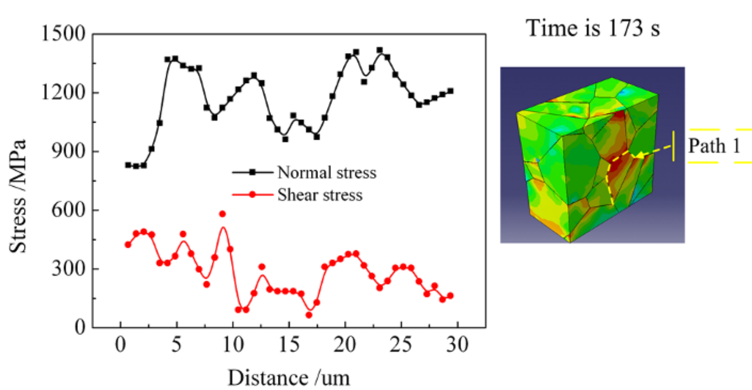

Figure 11: Normal stress and shear stress along the path

The layout of the S11 stress generated by the calculation on the voronoi polycrystal finite element model is shown in Fig.10. In the figure, as the load continues, the internal stress increases observably, especially at the grain boundaries there is evident stress concentration. The maximal S11 stress at the grain boundary is 1400 MPa, which is evidently higher than the S11 stress value at the crack tip, which is 1375 MPa. This can well explain the occurrence of multiple tiny cracks on the tip of main crack origins and their location at the grain boundaries. When time is set at 173 s, the evident failure of polycrystal occurs. As the SEM picture of in-situ test observation indicates in Fig.10, understandably, the stress concentration at the grain boundary area is the driving force of its crack initiation and expansion, while the energy is consumed by this in the area lowered the integral internal energy in this micro-area (range from 10 μm to 30 μm). Select path 1 on the polycrystal finite element model according to the area of stress concentration; and extract normal stress and shear stress at the path nodes as it is shown in Fig.11. Based on this it can be concluded that the driving force that leads to the fracture in heat affected zone are primarily the normal stress and peripherally shear stress. Meanwhile, at the same path, the shear stress value is approximately one third of the normal stress. This phenomenon exists in the research of CuW alloy by Wang Y.L [Wang, Liang and Ren (2012)]. The driving force for the fracture at the grain boundary is combined effect of the normal stress and the shear stress.

5 Conclusions

This experiment acquires the fracture criteria at the weakest zone in the Ti-6Al-4V titanium alloy welded joints (heat affected zone) through the in-situ tension method and finite element model. During the simulation, the GTN model is used to describe the damage behavior of the titanium alloy. The following conclusions can be drawn:

1) Based on previous research on the titanium alloy and other works, variable parameters used in the damage model were listed as: q_1=1.5; q_2=1; $q_3=q_1^2$=2.25; f_0=0.00058; f_f=0.08; f_c=0.005; ε_N=0.3; S_N=0.1.

2) By comparing the applied force between simulation of global model and in-situ test, the fracture criteria are discussed. The criterion is listed as: the critical stress is 1375 MPa; the critical fracture strain is 0.136; and the critical stress triaxiality is 2.33.

3) Based on the in-situ tensile test and its simulation, we conduct research on the fracture driving force under RVE model. The simulation result indicates that the driving forces for metal fracture are jointly from the normal stress and shear stress.

Acknowledgements

This project got the great support from National Fund of Natural Science (50875200), and the Ph.D. Programs Foundation of Ministry of Education of China (20100201110065). Here by Appreciate!

Reference

ABAQUS Theory Manual, Hibbitt, Karlsson. Sorensen. Inc., 1998.

Belytschko, T.; Black, T.(1999): Elastic Crack Growth in Finite Elements with Minimal Remeshing. *International. Journal. Numerical. Methods. Engineering.*, vol. 45, pp. 601-620.

Bao, G.; Hutchinson, J.W.; McMeeking, R.M.(1991): Particle reinforcement of ductile matrices against plastic flow and creep. *Acta. Metallurgica. Materialia.*, vol.39, no. 8, pp. 1871-1882.

Christman, T.; Needleman, A.; Suresh, S.(1989): An experimental and numerical study of deformation in metal-ceramic composites. *Acta. Metallurgica.*, vol.37, no. 11, pp.3029-3050.

Chan, K.S.; Kim, Y.S. (1995): Effects of lamellae spacing and colony size on the fracture resistance of a fully-lamellar TiAl alloy. *Acta. Mater.*, vol. 43, pp. 439-451.

Chen, J.H.; Cao, R.; Wang, G.Z. (2004): Study on notch fracture of TiAl alloys at room temperature. *Metall. Mater. Trans. A.*, vol.35, pp. 439-456.

Chen, J.H.; Wang, Q.; Wang, G.Z.; Li, Z. (2003): Fracture behavior at crack tip — a new framework for cleavage mechanism of steel. *Acta. Mater.*, vol.51, pp. 1841–1855.

Dong, L.; Atluri, S. N.(2011b): Development of T-Trefftz four-node quadrilateral and Voronoi Cell Finite Elements for macro- &micromechanical modeling of solids. *CMES. Computer. Modeling. Engineering. Science.*, vol.81, pp.69-118.

Dong, L.; Atluri, S. N.(2012a): T-Trefftz Voronoi Cell Finite Elements with eastic/rigid inclusions or voids for micromechanical analysis of composite and porous materials. *CMES. Computer. Modeling. Engineering. Science.*, vol.83, pp.183-220.

Dong, L.; Atluri, S. N.(2012b): A simple multi-source-point Trefftz method for solving direct/Inverse SHM problems of plane elasticity in arbitrary multiply-connected domains. *CMES. Computer. Modeling. Engineering. Science.*, vol.85, pp.1-44.

Dong, L.; Atluri, S. N.(2013a): SGBEM Voronoi Cells (SVCs), with Embedded Arbitrary-Shaped Inclusions, Voids, and/or Cracks, for Micromechanical Modeling of Heterogeneous Materials. *CMC. Computers. Materials. Continua.*, vol.33, pp.111-154.

Dong, L.; Atluri, S. N.(2013b): Fracture & Fatigue Analysis: SGBEM-FEM or XFEM? Part 1: 2D Structure. *CMES. Computer. Modeling. Engineering. Science.*,vol. 90, no. 2, pp. 91-146.

Gao, X.L.; Zhang, L.J.; Liu, J.; Zhang, J.X. (2013): A comparative study of pulsed Nd:YAG laser welding and TIG welding of thin Ti6Al4V titanium alloy plate. *Mater. Sci. Eng. A.*, vol. 559, pp. 14– 21.

Gurson, A.L. (1977): Continuum theory of ductile rupture by void nucleation and growth. Part I: yield criteria and flow rules for porous ductile media. *J. Eng. Mater.technol.*, vol. 99, pp. 2-15.

Hauert, A.; Rossoll, A.; Mortensen, A. (2010): Fracture of high volume fraction ceramic particle reinforced aluminium under multiaxial stress. *Acta. Materialia*,. vol. 58, pp. 3895–3907.

Lee, H.S.; Yoon, J.H.; Park, C.H.; Ko, Y.G.; Shin, D.H.; Lee, C.S. (2007): A study on diffusion bonding of superplastic Ti–6Al–4V ELI grade. *Journal. Materials. Processing. Technology.*, vol.187-188, pp. 526-529.

Murakawa, H.; Deng, D.A.; Ma, N.; Wang, J.C. (2011): Applications of inherent strain and interface element to simulation of welding deformation in thin plate structures. *Computational. Materials. Science.*, vol. 51, pp. 43-52.

Melenk, J.;Babuska, I.(1996): The Partition of Unity Finite Element Method: Basic Theory and Applications, *Computer. Methods. Applied. Mechanics. Engineering.*, vol. 39, pp. 289-314.

Moës, N; Dolbow J; Belytschko, T.(1999): A finite element method for crack growth without remeshing. *International. Journal. Numerical. Methods. Engineering.*, vol. 46, pp. 131-150.

Needleman, A.; Tvergaard, V. (1984): An analysis of ductile rupture in notched bars. *Journal. Mechanics. Physics. Solids.* vol. 32, pp. 461-490.

Osovski, S.; Nahmany, Y.; Rittel, D.; Landaub, P.; Venkert, A. (2012): On the dynamic character of localized failure. *Scripta. Mater.*, vol. 67, pp. 693-695.

Patankar, S.N.; Escobedo, J.P.; Field, D.P.; Salishchev, G.; Galeyev, R.M.; Valiakhmetov, O.R. (2002): Superior superplastic behavior in fine-grained Ti–6Al–4V sheet. *Journal. Alloys. Compounds.*, vol. 345, pp. 221-227.

Squillace, A.; Prisco, U.; Ciliberto, S.; Astarita, A. (2012): Effect of welding parameters on morphology and mechanical properties of Ti-6Al-4V laser beam welded butt joints. *Journal. Materials. Processing. Technology.*, vol. 212, pp. 427-436.

Tvergaard, V.; Needleman, A. (1984): Analysis of the cup-cone fracture in a round tensile bar. *Acta. Metall.*, vol. 32, pp. 157-169.

Ueda, Y.; Yuan, G.M.; Mochizuki, M.; Umezawa, S.; Enomoto, K. (1993): A prediction method of welding residual stress using source of residual (report IV)-experimental verification for prediction method of welding residual stresses in T-joints using inherent strains. *Trans. JWRI.*, vol. 26, pp. 169-176.

Wang, G.Z.; Liu, Y.G.; Chen, J.H. (2004): Investigation of cleavage fracture initation in notched specimens of a C-Mn steel with carbides and inclusions. *Mater. Sci. Eng. A.*, vol. 369, pp. 181-191.

Wang, R.; Zhang, J.X.; Serizawa, H.; Murakawa, H. (2009): Investigation of inherent deformation in fillet welded thin plate T-joints based on interactive substructure and inverse analysis method. *CMES. Computer. Modeling. Engineering. Science.*, vol.44, pp. 97-113.

Wang, Y.L.; Liang, S.H.; Ren, J.T.(2012): Analysis of meso-scale damage and crack for CuW alloys induced by thermal shock. *Mater. Sci. Eng. A.*, vol.534, pp. 542-546.

Zhang, J.X.; Song, X.; Zheng, L. (2012): Investigation into plastic damage behavior of the CO2 laser deep penetration welded joint for Ti–6Al–4V alloy. *Engineering. Fracture. Mechanics.*, vol. 83, pp. 1-7.

Zhao, X.L.; Zhang, J.X.; Song, X. (2012): In-situ investigation on mechanical behavior of laser-welded joint for TC4 titanium alloy. *Chinese. Journal. Nonferrous. Metals.*, vol. 22, pp. 388-393.

Zhao, X.L.; Zhang, J.X.; Guo, W. (2011): Estimating on the mechanical properties of laser welded joint of TC4 alloy with a shear punch testing. *Trans. JWRI.*, vol. Special issue on WSE2011, pp. 169-170.

Zhao, X.L.; Zhang, J.X.; Song, X.; Guo, W. (2013): Investigation on mechanical properties of laser welded joints for Ti–6Al–4V titanium alloy. *Materials. Science. Technology.*, in press.

Zhang, K.R.; Zhang, J.X. (2009): Numerical simulation for keyhole profile effect of TC4 titanium alloy during laser welding. *Rare. Metal. Materials. Engineering.*, vol.38, pp. 987-990.

Zhang, J.X.; Song, X.; Zheng, L. (2012): Study on nonlinear evolution of CO2 laser deep penetration welded joint for TC4 tittanium alloy. *Rare. Metal. Materials. Engineering.*, vol. 41, pp. 607-611.

Zhao, X.L.; Zhang, J.X. (2013): Small Punch Test of U-Shaped Notch of TC4 Titanium Alloy and Its Numerical Simulation. *Journal. Materials. Engineering. Performance.*, in press.